arXiv:2207.00865v1 [cs.CV] 2 Jul 2022

ORA3D: Overlap Region Aware Multi-view 3D Object Detection

Wonseok Roh[1], Gyusam Chang[1], Seokha Moon[3], Giljoo Nam[2]
Chanyoung Kim[1], Younghyun Kim[4], Sangpil Kim[1*], and Jinkyu Kim[3*]

[1]Department of Artificial Intelligence, Korea University
[2]School of Computing, KAIST
[3]Department of Computer Science and Engineering, Korea University
[4]Autonomous Driving Center, Hyundai Motor Company R&D Division
[*]Corresponding Authors

Abstract. In multi-view 3D object detection tasks, disparity supervision over overlapping image regions substantially improves the overall detection performance. However, current multi-view 3D object detection methods often fail to detect objects in the overlap region properly, and the network's understanding of the scene is often limited to that of a monocular detection network. To mitigate this issue, we advocate for applying the traditional stereo disparity estimation method to obtain reliable disparity information for the overlap region. Given the disparity estimates as a supervision, we propose to regularize the network to fully utilize the geometric potential of binocular images, and improve the overall detection accuracy. Moreover, we propose to use an adversarial overlap region discriminator, which is trained to minimize the representational gap between non-overlap regions and overlapping regions where objects are often largely occluded or suffer from deformation due to camera distortion, causing a domain shift. We demonstrate the effectiveness of the proposed method with the large-scale multi-view 3D object detection benchmark, called nuScenes. Our experiment shows that our proposed method outperforms the current state-of-the-art methods.

Keywords: Multi-view 3D Object Detection, Stereo Disparity Estimation, Multi-view Cameras

1 Introduction

Object detection, one of the fundamental problems of computer vision, has been widely conducted, and various methods are being introduced. Especially object detection in 3D space plays a crucial part while autonomous driving systems, robotics, and other real-world applications. Recent works using modalities like LiDAR and RADAR show promising results in detection tasks, including monocular [48,49,7,42] and stereo [28,11,13] tasks. While these modalities benefit from utilizing 360-degree view details, information about all static and dynamic objects like stationary pedestrians and moving vehicles can be sufficiently obtained

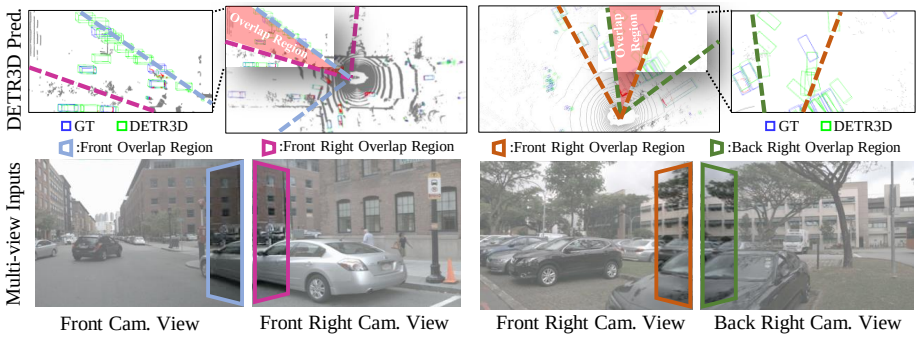

Fig. 1: Examples where DETR3D [47] fails to detect objects in the overlapped regions (see dotted line), resulting in performance degradation due to multiple false positives. The first row represents the BEV view of the two scenes in the second row. There are significantly more false positives in the overlapped regions than in others. The second row shows overlapped regions between multi-view images used as input to the network.

from multi-view images. In this paper, we tackle the object detection task in 3D space, which detects instances of specific classes with multi-view images input.

Most state-of-the-art 3D object detection methods [14,39,6,40,29] based on point clouds obtained from LiDAR yield reliable results but demand a large budget to establish LiDAR per vehicle. Meanwhile, methods [44,43,47,22] using single monocular images have cost advantages but require further performance improvement due to insufficient clues. Stereo detection methods [26,5,46,21] result in better performance with accurate depth estimation than monocular detection. However, there are still limitations in positioning stereo pairs in all directions on moving vehicles. Multi-view images taken around the ego vehicle make up for the weaknesses of monocular and stereo images. It also replaces meaningful role of a LiDAR with low burden.

Although depth estimation significantly impacts 3D object detection, accurate depth estimation from a single image remains challenging. Existing methods, including FCOS3D [44] and PGD [43], used a geometric approach to increase performance in monocular depth estimation. However, there is a problem that the depth is not expressed adequately on the pixel (e.g., inability to handle distant objects on pixels and depth compounding error properly). To avoid depth compounding errors, DETR3D [47] proposes a transition between 2D observation and 3D predictions, not relying on dense depth prediction. DETR3D is a multi-view detection model that processes six images as end-to-end learning that predicts all objects at once and utilizes set-based global loss. This method uses information from multiple cameras by back projecting 3D points on a 2D plane. It also characterizes by no additional post-processing stages, such as non-maximum suppression (NMS). Although DETR3D performs well, we have found that the network may not be guided to fully utilize the geometric potential of binocular images without explicit guidance. That is, the network's understand-

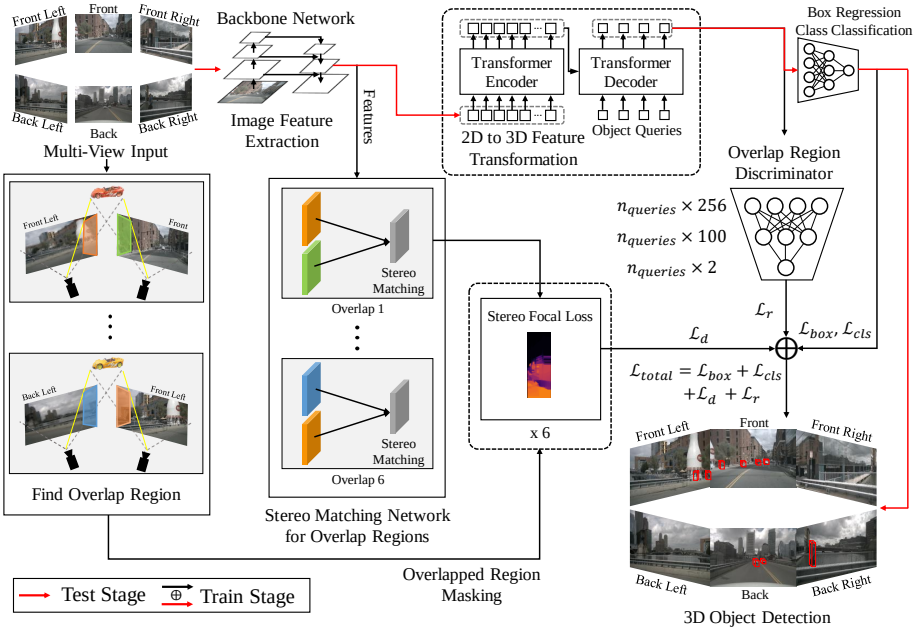

Fig. 2: An overview of our proposed architecture. Built upon DETR3D [47], our model takes multi-view camera inputs and outputs a set of 3D bounding boxes for objects in the scene. Our model consists of two main modules: (1) Stereo Matching Network for Overlap Regions, where our depth estimation head is trained to predict a dense depth map of the overlap region. The ground-truth depth map is obtained by a traditional stereo disparity estimation algorithm. (2) Adversarial Overlap Region Discriminator, which minimizes the gap between non-overlap regions vs. overlap regions, improving the overall detection performance.

ing of the scene could be limited to that of a monocular detection network, generating multiple false positives in the overlapped regions, as shown in Fig. 1.

To mitigate this issue, we advocate for explicitly leveraging the depth information from multiple cameras with overlapping Field Of View(FOV). This is due to the fact that the stereo-view contains more information than the mono-view, yielding a reliable depth estimation performance via well-studied stereo disparity estimation techniques. Given the intrinsic and extrinsic of multiple cameras, we first find the accurate overlap region and obtain outputs from the traditional stereo disparity estimation model on the overlap region. We, then, use them as a supervision to regularize the image feature extraction backbone and to improve the overall detection accuracy for objects across overlapped cameras. We empirically observe that regularizing with even a small overlap region ($\approx 20\%$ of the total region) substantially improves the detection performance. An overview of our proposed model architecture is shown in Fig. 2.

This is only part of a story. Unlike the human vision system that easily identifies an object across overlapped cameras, we empirically found that DNN has a

strong inductive bias towards identifying objects individually in each image, failing to utilize rich information from the overlap region. Thus, we further propose to train an adversarial overlap region discriminator, which explicitly minimizes the gap between objects in the non-overlap regions vs. overlap regions. Our experiment results show that such adversarial training improves the overall object detection performance.

As shown in Fig. 2, we start from the state-of-the-art model of multi-view modality, called DETR3D [47], which is established on a transformer-based object detection head given representations of 360° surround images. Built upon DETR3D, we propose to use the following two main modules: (i) Stereo Disparity Estimation for Supervision and (ii) Adversarial Overlap Region Discriminator. We evaluate the effectiveness of our proposed method using nuScenes [1] dataset, which is a widely-used large-scale multi-view 3D object detection benchmark. Our experiments show that our proposed model generally outperforms the state-of-the-art approaches in the camera-only 3D object detection task. Our main contributions are summarized as follows:

- We propose an overlap region discriminator which is optimized by using adaptation loss to obtain robust performance in overlap region by fooling the network to recognize the actual overlap regions are not from the original overlapped area domain.
- We introduce a novel method that approximates the 3D geometric information of the scene for 3D object detection by utilizing a stereo matching on the overlap region, which drastically improves the performance of the 3D object detection network.
- We identify that the objects in the edges of the views and their redundant appearance in neighbor views are the major problem of the performance drawback in the conventional multi-view-based 3D object detection methods.

2 Related Work

2D Object Detection. After the advent of deep learning, R-CNN [10] is an early object detection model applied Convolution Neural Network (CNN). Although the model achieved impressive performance improvement by proposing bottom-up region proposals, it consumes a considerable amount of time due to excessive convolution computations. To address this problem, Fast R-CNN [9] introduced a sharable ConvNet structure with a single forward pass. And Faster R-CNN [34] achieved remarkable time savings by embedding the region proposal module in the network. However, existing two-stage detectors that perform region proposals and classification sequentially still require vast resource. YOLO [33] and SSD [25], which are single-stage detectors, break away from the existing non-optimal two-stage structure and present an end-to-end pipeline using a single neural network. CenterNet [53] and FCOS [41] suggest a new paradigm that does not require post-processing using a pixel-based prescription

method rather than a predefined anchor box method. DETR [2] introduces a method of recognizing object detection as a direct set prediction problem.

3D Object Detection. As research to infer objects in 3D plane begins, Mono3D [4] conducts 3D object detection task using multiple information such as RGB images, object instruction segmentation, context, and location prior information. The model proposed by Roddick, T. *et al.* [35] utilizes Bird-Eye-View(BEV) to compensate for performance degradation by incorrect depth feature extracted from solely RGB images. MonoPSR [19] presents a method to significantly reduce 3D search space using 2D object detection and exploit point clouds to recover local shape and scale. FCOS3D [44] and RTM3D [22] predicts 3D bounding box more accurately through features guided by geometric information. In addition, PGD [43] shows that geometric interactions between objects enhance the reliability of depth. Yet, the methods mentioned above perform detection tasks independently for each image. Thus, to expand for multiple cameras, each frame processing is performed before integrating the outputs in the post-processing stage. To address this problem, DETR3D [47] introduces a 3D object detection method that simultaneously processes multi-view images. DETR3D predicts 3D bounding boxes via backward geometric projection and operates set-to-set prediction without post-processing. Recently, ImVoxelNet [36] implements a surrounding view 3D object detector similar to the LiDAR system by optimizing the chronic computation of multiple images. Although they use multi-view images as input, they do not take advantage of the features of multiple camera settings. Therefore, our proposed method focuses on overlaying clues between images, which are multi-view characteristics, to improve detection performance.

Stereo 3D Object Detection. The stereo 3D object detection task that utilizes binocular information is similar to the human system. Inspired by depth estimation models [51,18,3] that utilize the rich geometric features provided by stereo views, DSGN [5] proposes an end-to-end model that simultaneously uses plane-sweep volume and 3D geometric volume to predict 3D bounding boxes. PLUMEnet [46] directly constructs a pseudo-LiDAR feature volume (PLUME) in 3D space, which solves both depth estimation and object detection tasks. Reliable depth features extracted from the stereo view yield outstanding performance, whereas the 3D cost volume formed in the stereo network directs a lot of computation complexity. YOLOStereo3D [26], a single-stage 3D detection network, effectively deals with the trade-off between computational complexity and depth accuracy with lightweight cost volume. Additionally, MobileStereoNet [38] introduces a way to leverage MobileNets [16] to reduce the computation cost of deep networks without sacrificing accuracy. From these observations, our method utilizes the disparity information as 3D geometric cues in multi-view settings to enhance the detection performance for the multi-view-based 3D object detection.

Pseudo-Lidar Methods. Existing image-representation methods suffer from pixel distortion and low-resolution issues for distant objects. Wang, Y. *et al.* [45] presents Pseudo-LiDAR to overcome the expressive limitations of RGB images. After that, Pseudo-LiDAR++ [50] leads to performance improvement through extremely sparse LiDAR sensors and stereo depth estimation with improved per-

formance. Previous works in which depth map extraction and 3D point cloud conversion occur separately induce suboptimal performance. To address this, Qian, R. *et al.* [32] builds an end-to-end pipeline using the Change of Representation (CoR) module. Recently, Liu, H. *et al.*emphasizes the importance of interpolation and suggests an efficient multi-modal deep aggregation module [24]. However, the massive computation of the network exploiting point clouds and the demand for pricey resources of LiDAR modality remain challenges.

3 Method

We propose a multi-view 3D object detection model that leverages rich information from a multi-view vision system. Our model is built upon the state-of-the-art DETR3D [47] model, which takes RGB images from a set of multi-view cameras and outputs a set of 3D bounding boxes for objects in the scene. Note that we assume that the intrinsic and extrinsic of cameras are known.

As we empirically found that DETR3D often exhibits a failure to detect objects in the overlap region, we propose to use the following main modules to address this issue:

1. Stereo Disparity Estimation for Supervision. As reported by Chen *et al.* [5], disparity supervision substantially improves the detection performance. Without such disparity supervision, the network may not be guided to completely utilize the geometric potential of binocular images, and the network's understanding of the scene could be limited to that of a monocular detection network. Thus, we want to use outputs from the traditional stereo disparity estimation model on the overlap region and apply them as a weak supervision to improve the detection accuracy over the overlap region. We empirically observe that this supervision significantly improves the overall detection accuracy.

2. Adversarial Overlap Region Discriminator. We further explore the adversarial overlap region discriminator, which is adversarially trained to minimize the gap between non-overlap regions vs. overlap regions. We empirically observe that objects on the overlap region are often largely occluded (or cropped), causing a domain shift.

In the following sections, we first briefly review the state-of-the-art DETR3D model (Section 3.1) and explain how we improve it by leveraging information from the overlap region of a set of multi-view images (Section 3.2 and Section 3.3).

3.1 DETR3D

We extend the previous state-of-the-art DETR3D [47] to perform multi-view 3D detection. DETR3D, which is motivated by DETR [2], predicts the 3D coordinates of a set of queries directly in 3D space and has an NMS-free structure, unlike existing 3D object detection models. DETR3D uses multi-view images as input and yields more promising performance than mono modality, even in multi-view modality that processes six images simultaneously. Multi-view images

also have the advantage of using 360-degrees views, and some overlap regions allow more useful depth information through stereo matching. Therefore, our study uses a network that employs information in an overlap region based on DETR3D.

3.2 Stereo Disparity Estimation for Supervision

Since the stereo view contains more information than the mono view, it yields excellent performance in depth estimation and 3D reconstruction tasks. However, unlike typical stereo datasets KITTI stereo [8,30,37], the nuScenes dataset [1] has a small overlapping area because the cameras that collect images are installed to look at different directions. In this section, we present a method to effectively utilize such small but effective information.

Overlap Region Definition.

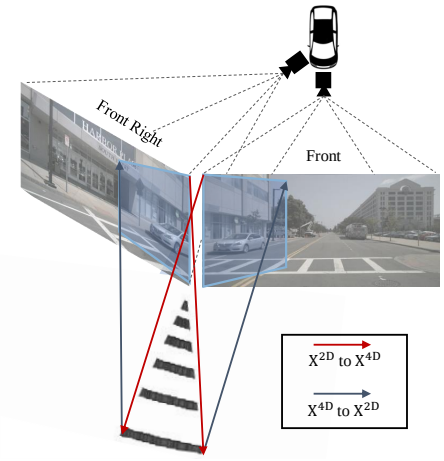

Fig. 3: Overview of finding the overlap region between the front and the front right camera.

As shown in Fig. 3, our model finds the accurate overlap region using projection matrices collected from each camera in six multi-view images. The process of finding the exact overlap region is the basis of our model. Our method starts with a set of six images for $I = \{\mathbf{i}_f, \mathbf{i}_{fr}, \ldots, \mathbf{i}_{br}\} \in \mathbb{R}^{H \times W \times 3}$ and combinations of camera intrinsics and extrinsics. The actual overlap region between the two cameras depends on the scene depth. In order to get the accurate overlapping pixels, we apply an infinite value d_∞ to the scene depth. The process of converting to 3D coordinates by applying infinite depth to the 2D coordinates of $\mathbf{X}_f^{2D} = [u,\ v]$, which is expected to be the right overlap region of the front camera, is described below.

$$\mathbf{X}_i^{3D} = [u\ \times d_\infty,\ v \times\ d_\infty,\ d_\infty] \tag{1}$$

$\mathbf{X}_f^{3D}$ represents the 3D representation of $\mathbf{X}_f^{2D}$. We convert 4D by concatenating 1 to $\mathbf{X}_f^{3D}$ as below in order to multiply it with a transformation matrix having a 4x4 shape.

$$\mathbf{X}_f^{4D} = \mathbf{X}_f^{3D} \oplus 1 \tag{2}$$

Then multiply the transformation matrices $T = \{\mathbf{T}_f, \mathbf{T}_{fr}, \ldots, \mathbf{T}_{br}\} \in \mathbb{R}^{4\times4}$ to convert camera coordinates $\mathbf{X}_f^{4D}$ into the egocentric coordinates.

$$\mathbf{X}_f^{\text{ego}} = \mathbf{T}_f\ \cdot\ \mathbf{X}_f^{4D} \tag{3}$$

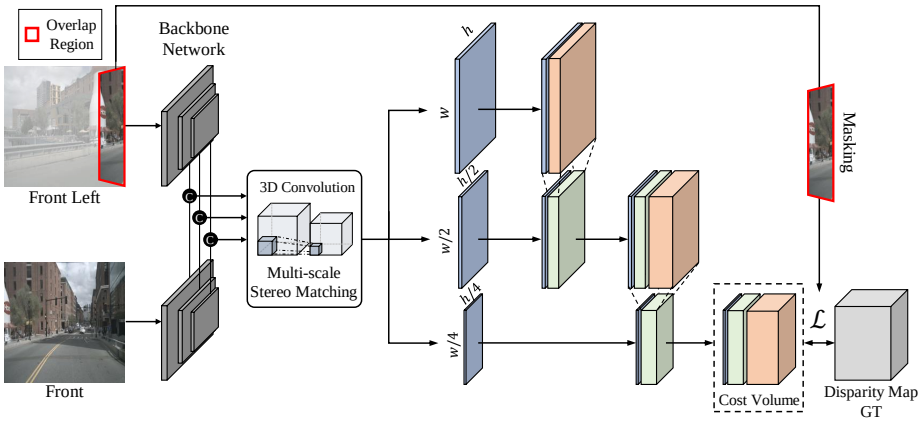

Fig. 4: Stereo disparity estimation head architecture. The overlap regions of the left and right images are downsampled by four and input to the network; the shape is [B, C, H, W], respectively. Left and right data are concatenated in the network to form a cost volume through 3D convolution layer. As a result, the estimated cost volume is used in the loss calculation.

New transformation matrices are needed to translate the LiDAR coordinates into camera space. Since it is a transformation from the egocentric to the camera in the reverse direction, the existing inverse matrix of T is utilized. As shown in below, we multiply $\mathbf{T}_{fr}^{-1}$ to convert $\mathbf{X}_{f}^{\text{ego}}$ into front right camera space.

$$\mathbf{X}_{fr}^{*4D} = \mathbf{T}_{fr}^{-1} \cdot \mathbf{X}_{f}^{\text{ego}} \tag{4}$$

Finally, we divide by the depth d_X in pixels to project the front camera completely into the front right camera.

$$\mathbf{X}_{fr}^{4D} = \mathbf{X}_{fr}^{*4D} \; / \; d_X \tag{5}$$

Through the above formulas, it is possible to find the accurate overlap region between two cameras.

Multi-view Stereo Matching. Given disparity supervision over the overlapped areas, we train our Stereo Disparity Estimation head to reconstruct a dense disparity map with stereo features. As shown in Fig. 4, multi-view images are first processed by 2D feature extractors based on residual network architecture. A pair of the resulting feature tensors for the overlapped area is collected from each pair of neighboring cameras. Then stereo feature pairs are fed into the stereo disparity estimation head to obtain a dense disparity map.

To implement the disparity estimation head, we closely follow the recent work by Liu *et al.* [26]. Our model utilize the pixel-wise correlation module to learn rich stereo representations and fuse multi-scale hierarchical stereo features to estimate the disparity map densely. Note that our disparity estimation module is supervised only for the overlapped areas, but we empirically exhibit that it significantly improves the network's overall 3D object detection performance.

Further, our disparity estimation head can be disabled during evaluation and testing to improve computational efficiency. More implementation details are provided in the supplemental material.

Stereo Disparity Estimation Loss. We use a standard stereo focal loss [52] on the disparity estimation from a pair of overlapped images. Using the output of the stereo matching algorithm [15] as a supervision, we optimize the following stereo focal loss to train our Stereo Disparity Estimation head:

$$\mathcal{L}_d = \frac{1}{|\mathcal{P}|} \sum_{p \in \mathcal{P}} \sum_{d=0}^{D-1} ((1 - P_p(d)))^{-\alpha} (-P_p(d) \log \hat{P}_p(d)) \tag{6}$$

where d and D denote predicted disparity and max-disparity, respectively. α is the focus weight. $P_p(d)$ and $\hat{P}_p(d)$ represent the expected and predicted distribution of disparity d for a set of overlapped pixels $p \in \mathcal{P}$. $P_p(d)$ is defined as follows: $P_p(d) = \text{Softmax}(-2|d - d^{gt}|)$ where d^{gt} is the target (or ground-truth) disparity map.

3.3 Adversarial Overlap Region Discriminator

Unlike the human vision system that easily identifies an object appearing simultaneously in different-view images, we empirically found that DNN-based multi-view object detection models have a strong inductive bias towards identifying objects individually in each image. In particular, existing works often fail to leverage information of the overlap region effectively. Moreover, we also observe a domain shift effect between the overlap region (i.e. region far from camera center) vs. non-overlap region (i.e. region near camera center). Objects in the overlap region are often largely occluded due to limited FOV of the camera or suffer from deformation due to camera lens distortion (e.g. pincushion distortion).

In addition to leveraging stereo disparity information, which gives an implicit bias to process the same object in different-view images together, we propose to use a regularizer to explicitly minimize the representational gap between non-overlap regions vs. overlapping regions. Specifically, we constrain the object detection head from learning region-invariant information via an adversarial framework using *gradient reversal layer* (GRL).

Formally, given a query feature $\mathbf{q}_i$ for $i = \{1, 2, \ldots, |Q|\}$ in the transformer (i.e. object detection decoder), an overlap region discriminator f_d takes such query features and it needs to predict its source region correctly. Thus, this classifier f_d is trained using region classification loss $\mathcal{L}_r$ as follows:

$$\mathcal{L}_r = -\mathbb{E}_{q, y_r \sim \mathbb{D}} \left[\sum_{r \in \mathcal{R}} y_r \log f_d(q)_r \right] \tag{7}$$

where $\mathbb{E}_{q, y_r \sim \mathbb{D}}$ indicates an expectation over samples (q, y_r), which are drawn from the (input) data distribution $\mathbb{D}$. Plus, f_d is trained to classify whether

a query feature is from the overlap region (y_r is set to 1) or from the non-overlap region (y_r is set to 0), so the output dimension from this module is 2 (i.e. $y_r \in \{0, 1\}$). Our encoder is then trained by minimizing the following adversarial loss, i.e. $-\mathcal{L}_r$.

Loss Function. Ultimately, our model is trained end-to-end by minimizing the following loss function $\mathcal{L}_{\text{total}}$:

$$\mathcal{L}_{total} = \lambda_{\text{cls}}\mathcal{L}_{\text{cls}} + \lambda_{\text{box}}\mathcal{L}_{\text{box}} + \lambda_d\mathcal{L}_d - \lambda_r\mathcal{L}_r \tag{8}$$

where λ_{cls}, λ_{box}, λ_d, and λ_r are hyperparameters that are drawn from a grid search to control the strength of λ_{cls}, $\mathcal{L}_{\text{box}}$, $\mathcal{L}_d$, and $\mathcal{L}_r$, respectively.

4 Experiments

4.1 Implementation and Evaluation Details

Dataset. We use nuScenes [1] dataset, which is a large-scale multi-view object detection benchmark. nuScenes dataset provides a full 360-degree field of view captured by 6 differently-viewing cameras. This comprises 20-second-long 1,000 video sequences, which are fully annotated with 3D bounding boxes for 10 object classes. The dataset covers 28k annotated samples for training, and validation and test contain 6k scenes each. Note that we use the best-performed model on validation for evaluation.

Evaluation Metrics. We follow the official evaluation protocol of nuScenes [1]. We use a set of True Positive metrics (TP metrics) for each prediction that was matched with a ground-truth box. We employ the following 5 TP metrics: Average Translation Error(ATE), Average Scale Error(ASE), Average Orientation Error(AOE), Average Velocity Error(AVE), and Average Attribute Error(AAE). All TP metrics are also calculated using a 2m center distance threshold during matching, and they are all designed to be positive scalars. We also measure mean average precision (mAP). Lastly, we use the nuScenes Detection Score (NDS) to measures a consolidated scalar metric defined as follows:

$$\text{NDS} = \frac{1}{10}[5\ \text{mAP} + \sum_{\text{mTP}\in\mathbb{TP}} (1 - \min(1, \text{mTP}))] \tag{9}$$

where $\mathbb{TP}$ is five TP metrics.

Network Architectures. Our model is built upon DETR3D [47] architecture. We use ResNet101 [12] as the feature extraction backbone followed by Feature Pyramid Networks (FPN) [23] to generate multi-level predictions based on the input images. Note that the transformer-based detection head consists of 6 layers, each of which uses a combination of feature improvement stages and multi-head attention layers.

Training Details. Following the default setting used by DETR3D, our model is trained end-to-end using AdamW [27] as an optimizer with the learning rate 3e-5. Our model is initialized from the DETR3D checkpoint and is trained for 30

Table 1: Comparing our 3D object detector and the state-of-the-art on the nuScenes [1] dataset. All methods based on camera modality. † : trained with CBGS [54]. ∗ : initialized from pre-trained model on extra data. ‡ : initialized from DD3D checkpoint.

Model	Mono|Multi	Backbone	NDS(↑)	mAP(↑)
CenterNet [53]	Mono	DLA34	0.328	0.306
FCOS3D [44]	Mono	ResNet101	0.415	0.343
PGD [43]	Mono	ResNet101	0.428	0.369
DETR3D [47]	Multi	ResNet101	0.425	0.346
DETR3D † [47]	Multi	ResNet101	0.434	0.349
Ours	Multi	ResNet101	**0.441**	**0.364**

(a) Validation set.

Model	Mono|Multi	Backbone	NDS(↑)	mAP(↑)
FCOS3D [44]	Mono	ResNet101	0.428	0.358
PGD [43]	Mono	ResNet101	0.448	0.386
DD3D ∗ [31]	Mono	V2-99	0.477	0.418
DETR3D ‡ [47]	Multi	V2-99	0.479	0.412
BEVDet ‡ [17]	Multi	V2-99	0.482	0.422
Ours ‡	Multi	V2-99	**0.489**	**0.423**

(b) Test set.

Table 2: Average precision (AP) for each object class on the nuScenes [1] test set. Higher value is better. *Abbr.* C.V: construction vehicle, Ped.: pedestrian, Motor.: motorcycle, T.C: traffic cone.

Model	Car	Truck	Bus	Trailer	C.V	Ped.	Motor.	Bicycle	T.C	Barrier	mAP
DETR3D [47]	0.603	0.333	0.290	0.358	0.170	0.455	0.413	0.308	0.627	0.565	0.412
Ours	**0.609**	**0.338**	**0.323**	**0.347**	**0.174**	**0.467**	**0.420**	**0.311**	**0.649**	**0.589**	**0.423**

epochs with four RTX 3090 GPUs. As the stereo disparity estimation network and adversarial overlap region discriminator are turned off during inference, the inference time would remain the same as that of DETR3D.

4.2 Quantitative Analysis.

3D Object Detection Performance against State-of-the-art. We compare our proposed method with existing state-of-the-art methods including CenterNet [53], FCOS3D [44], and DETR3D [47]. CenterNet and FCOS3D are mono image-based 3D object detection method, which needs to process each image independently to perform multi-view object detection. Thus, they emphasize less on scene geometry and sensor configuration. There proposed a few multi-view object detection approaches, and we compare ours to the current state-of-the-art DETR3D. As shown in Table 1 (a), our method generally outperforms other methods (compare the last row vs. others) in terms of (a consolidated metric) NDS and mAP. Note that FCOS3D uses test-time augmentation and a customized data augmentation strategy, thus requiring more epochs and model ensembles. Ours performs better than these methods even though we do not use any augmentation strategy.

In addition to offline results, we further report the detection performance on nuScenes [1] test set against recent state-of-the-art methods in Table 1 (b). Our highest-performance model, reinforced by the V2-99 [20] backbone, achieves a 0.489 NDS score and 0.423 mAP, overwhelming current state-of-the-art methods using the same backbone as ours. Note that we also initialized with DD3D [31] pre-trained model just like the others. As shown in Table 2, we also measure Average Precision (AP) of ours vs. DETR3D for each class on the nuScenes test

Table 3: Comparing our 3D object detector and the state-of-the-art for **objects in the overlap region**. Scores on the nuScenes [1] validation set are reported. All models use ResNet101 [12] as a backbone.

Model	Mono|Multi	NDS (↑)	mAP (↑)	mATE (↓)	mASE (↓)	mAOE (↓)	mAVE (↓)	mAAE (↓)
FCOS3D [44]	Mono	0.317	0.213	0.841	**0.276**	0.604	1.122	**0.173**
DETR3D [47]	Multi	0.356	0.231	0.825	0.280	0.400	0.863	0.223
Ours	Multi	**0.405**	**0.261**	**0.676**	0.284	**0.364**	**0.751**	0.183

set. Our method is initialized from the same checkpoint as DETR3D [47] and uses the same backbone for a fair comparison. Ours exhibits better performance in detecting all object classes.

3D Object Detection Performance against State-of-the-art on Overlap Region. We compare again our proposed method with existing state-of-the-art methods (FCOS3D [44], and DETR3D [47]), but here we focus only on overlap regions. As shown in Table 3, our method clearly outperforms FCOS3D and DETR3D in terms of all metrics except mASE and mAAE. Similar to the previous experiment, all models use ResNet101 as a backbone for a fair comparison and no augmentation is used except FCOS3D. This confirms that our overlap region aware approach is effective to deal with objects in the overlap region, resulting in a large performance gain.

4.3 Qualitative Analysis

Fig. 5 shows a visualization of 3D bounding boxes predicted by DETR3D (left column, see green boxes) and our proposed method (right column, see pink boxes). The ground-truth bounding boxes (see blue boxes) are overlaid. We project the predicted and ground-truth bounding boxes in the BEV perspective. In general, DETR3D and our proposed method generate reasonable results. However, the difference in the overlap region is apparent between the two methods, where DETR3D exhibits a relatively large number of false positive detections.

4.4 Ablation Study

We evaluate variants of our method with DETR3D with and without the following two main loss terms: (i) $\mathcal{L}_d$: Stereo Disparity Estimation loss, (ii) $\mathcal{L}_r$: Adversarial Overlap Region Discrimination loss. In Table 4, scores are reported on the nuScenes mini validation set (note that we chose this mini subset to reduce the computational burdens for this ablation study). We observe that adding either $\mathcal{L}_d$ improves all metrics except two metrics: mAVE and mAAE, while a similar trend is observed by adding $\mathcal{L}_r$ as well.

In Table 5, the effect of each component on the overlap region is verified. The stereo matching loss is reflected during backbone training, contributing to the performance improvement evenly in all areas without distinguishing between overlap and non-overlap regions. Our overlap region discriminator is a network

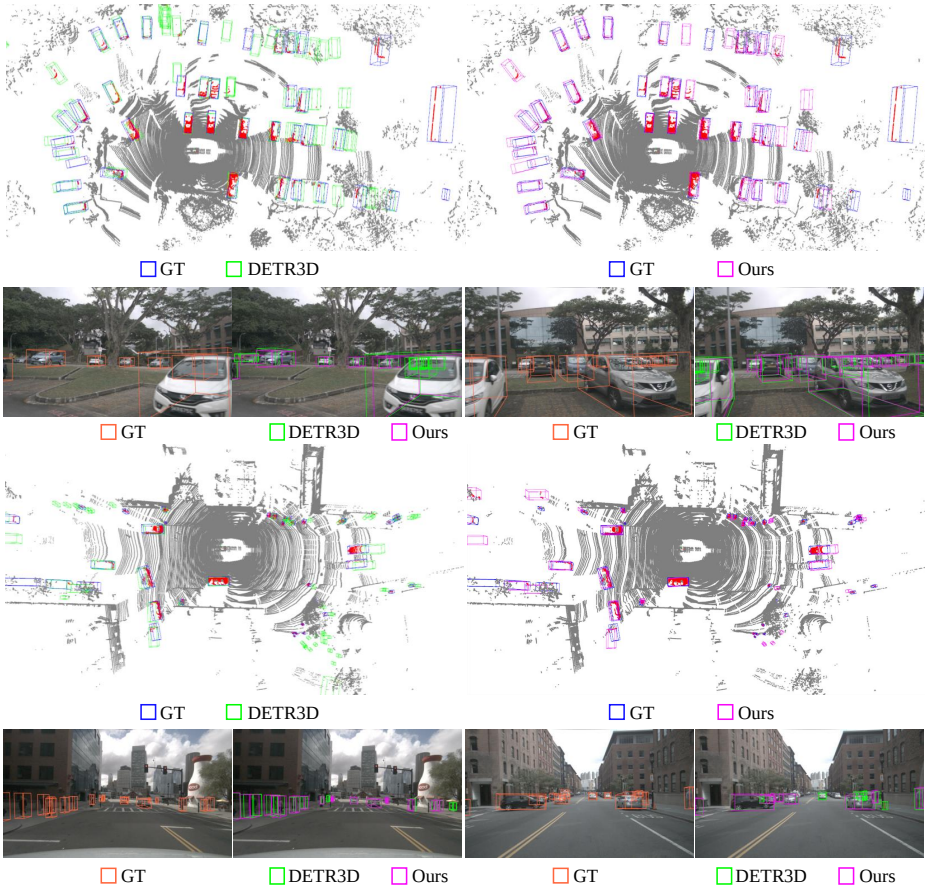

Fig. 5: Qualitative comparison between our method and previous state-of-the-art multi-view 3D object detection method DETR3D [47]. Each block describes the results of projecting 3D bounding boxes to the BEV perspective and projecting them to the image plane.

that overcomes performance differences by making it impossible for a model to discriminate whether it is an overlap region. In practice, we verify that the overlap region discriminator performs as intended in the overlap region rather than in the non-overlap area. The overlap region discriminator reduces the overall error and shows the same level of performance improvement as stereo matching in the overlap region.

5 Discussion

Here we discuss several exciting future research avenues that can address current limitations of our method. While the disparity estimation network outputs dense disparity maps for each view, we do not explicitly utilize the estimated

Table 4: Ablative analysis of our methods and DETR3D [47] on the nuScenes [1] *mini* validation set. All models use ResNet101 [12] as a backbone.

Model	NDS (↑)	mAP (↑)	mATE (↓)	mASE (↓)	mAOE (↓)	mAVE (↓)	mAAE (↓)
A. DETR3D [47]	0.338	0.247	0.917	0.468	0.674	**0.499**	**0.298**
B. A + $\mathcal{L}_d$	0.348	0.273	**0.805**	**0.454**	**0.598**	0.724	0.307
C. A + $\mathcal{L}_r$	0.339	0.286	0.831	0.455	0.693	0.756	0.309
D. A + $\mathcal{L}_d$ + $\mathcal{L}_r$ (Ours)	**0.353**	**0.288**	0.827	0.455	0.654	0.677	0.303

Table 5: Ablative analysis of overlap region on the nuScenes [1] *mini* validation set. All models use ResNet101 [12] as a backbone.

Model	NDS (↑)	mAP (↑)	mATE (↓)	mASE (↓)	mAOE (↓)	mAVE (↓)	mAAE (↓)
A. DETR3D [47]	0.266	0.151	0.900	0.550	0.731	**0.500**	**0.411**
B. A + $\mathcal{L}_d$	0.276	0.195	0.827	**0.549**	**0.689**	0.737	0.421
C. A + $\mathcal{L}_r$	0.274	**0.215**	**0.822**	**0.549**	0.775	0.773	0.422
D. A + $\mathcal{L}_d$ + $\mathcal{L}_r$ (Ours)	**0.280**	0.207	0.840	**0.549**	0.739	0.692	0.415

disparities for 3D object detection. We rather use the disparity estimation network as an intermediate medium that allows the image backbone network to extract 3D aware image features for overlapping regions as shown in Fig. 2. Although we have shown that such indirect guidance already adds performance improvement to the object detection head, explicit utilization of the estimated disparity maps or depth maps would give us better performance. As a future work, we would like to improve the performance of the stereo matching network and integrate the network with the object detection head for better utilization of the estimated disparities. As mentioned, instead of a dense depth map, we use a stereo disparity map obtained from the overlap region to utilize 3D information of the multi-view scenes for 3D detection network. This significantly improves the accuracy of the 3D detection pipeline. Therefore, there is plenty of room for performance improvement if the dataset contains the dense depth map to inform dense 3D geometric and uses the dense depth map to replace stereo disparity map estimation with dense map estimation on the overlap region. In terms of training computation complexity, many 3D object detection methods rely on CBGS [54] to improve the performance, regardless of increasing computation complexity approximately four times. However, our proposed method achieves state-of-the-art results without using CBGS method.

6 Conclusion

In this paper, we present methods to improve the performance of multi-view 3D object detection using the hint from small overlap regions. In the existing multi-view modality, the overlap region has become a weakness due to issues such as disconnected information and overlapping objects. However, the overlap region is also a novel material for improving overall performance. Our model applies the most specialized methods to reasonably utilize this small but very

informative region on detection and produces promising results. The first is a light and robust stereo disparity estimation network for small overlap regions. This network makes it possible to overcome the challenge of the overlap region. Next is the adversarial overlap discriminator, which is adversarially trained to minimize the gap between non-overlap regions and the overlapping regions. We empirically observe that our two methods significantly improve the overall detection accuracy. Furthermore, our methods of 3D object detection can be used in many other real-world applications, including autonomous driving systems.

Acknowledgements

This work is supported by Autonomous Driving Center, Hyundai Motor Company R&D Division.

References

1. Caesar, H., Bankiti, V., Lang, A.H., Vora, S., Liong, V.E., Xu, Q., Krishnan, A., Pan, Y., Baldan, G., Beijbom, O.: nuscenes: A multimodal dataset for autonomous driving. In: Proceedings of the IEEE/CVF conference on computer vision and pattern recognition. pp. 11621–11631 (2020)
2. Carion, N., Massa, F., Synnaeve, G., Usunier, N., Kirillov, A., Zagoruyko, S.: End-to-end object detection with transformers. In: European conference on computer vision. pp. 213–229. Springer (2020)
3. Chang, J.R., Chen, Y.S.: Pyramid stereo matching network. In: Proceedings of the IEEE conference on computer vision and pattern recognition. pp. 5410–5418 (2018)
4. Chen, X., Kundu, K., Zhang, Z., Ma, H., Fidler, S., Urtasun, R.: Monocular 3d object detection for autonomous driving. In: Proceedings of the IEEE conference on computer vision and pattern recognition. pp. 2147–2156 (2016)
5. Chen, Y., Liu, S., Shen, X., Jia, J.: Dsgn: Deep stereo geometry network for 3d object detection. In: Proceedings of the IEEE/CVF conference on computer vision and pattern recognition. pp. 12536–12545 (2020)
6. Deng, J., Shi, S., Li, P., Zhou, W., Zhang, Y., Li, H.: Voxel r-cnn: Towards high performance voxel-based 3d object detection. arXiv preprint arXiv:2012.15712 **1**(2), 4 (2020)
7. Dou, J., Xue, J., Fang, J.: Seg-voxelnet for 3d vehicle detection from rgb and lidar data. In: 2019 International Conference on Robotics and Automation (ICRA). pp. 4362–4368. IEEE (2019)
8. Geiger, A., Lenz, P., Urtasun, R.: Are we ready for autonomous driving? the kitti vision benchmark suite. In: 2012 IEEE conference on computer vision and pattern recognition. pp. 3354–3361. IEEE (2012)
9. Girshick, R.: Fast r-cnn. In: Proceedings of the IEEE international conference on computer vision. pp. 1440–1448 (2015)
10. Girshick, R., Donahue, J., Darrell, T., Malik, J.: Rich feature hierarchies for accurate object detection and semantic segmentation. In: Proceedings of the IEEE conference on computer vision and pattern recognition. pp. 580–587 (2014)
11. Guo, X., Shi, S., Wang, X., Li, H.: Liga-stereo: Learning lidar geometry aware representations for stereo-based 3d detector. In: Proceedings of the IEEE/CVF International Conference on Computer Vision. pp. 3153–3163 (2021)
12. He, K., Zhang, X., Ren, S., Sun, J.: Deep residual learning for image recognition. In: Proceedings of the IEEE conference on computer vision and pattern recognition. pp. 770–778 (2016)
13. He, Q., Wang, Z., Zeng, H., Liu, Y., Liu, S., Zeng, B.: Stereo rgb and deeper lidar based network for 3d object detection. arXiv preprint arXiv:2006.05187 (2020)
14. He, Q., Wang, Z., Zeng, H., Zeng, Y., Liu, S., Zeng, B.: Svga-net: Sparse voxel-graph attention network for 3d object detection from point clouds. arXiv preprint arXiv:2006.04043 (2020)
15. Hirschmuller, H.: Stereo processing by semiglobal matching and mutual information. IEEE Transactions on pattern analysis and machine intelligence **30**(2), 328–341 (2007)
16. Howard, A.G., Zhu, M., Chen, B., Kalenichenko, D., Wang, W., Weyand, T., Andreetto, M., Adam, H.: Mobilenets: Efficient convolutional neural networks for mobile vision applications. arXiv preprint arXiv:1704.04861 (2017)

17. Huang, J., Huang, G., Zhu, Z., Yun, Y., Du, D.: Bevdet: High-performance multi-camera 3d object detection in bird-eye-view. arXiv preprint arXiv:2112.11790 (2021)
18. Kendall, A., Martirosyan, H., Dasgupta, S., Henry, P., Kennedy, R., Bachrach, A., Bry, A.: End-to-end learning of geometry and context for deep stereo regression. In: Proceedings of the IEEE international conference on computer vision. pp. 66–75 (2017)
19. Ku, J., Pon, A.D., Waslander, S.L.: Monocular 3d object detection leveraging accurate proposals and shape reconstruction. In: Proceedings of the IEEE/CVF conference on computer vision and pattern recognition. pp. 11867–11876 (2019)
20. Lee, Y., Park, J.: Centermask: Real-time anchor-free instance segmentation. In: Proceedings of the IEEE/CVF conference on computer vision and pattern recognition. pp. 13906–13915 (2020)
21. Li, P., Chen, X., Shen, S.: Stereo r-cnn based 3d object detection for autonomous driving. In: Proceedings of the IEEE/CVF Conference on Computer Vision and Pattern Recognition. pp. 7644–7652 (2019)
22. Li, P., Zhao, H., Liu, P., Cao, F.: Rtm3d: Real-time monocular 3d detection from object keypoints for autonomous driving. In: European Conference on Computer Vision. pp. 644–660. Springer (2020)
23. Lin, T.Y., Dollár, P., Girshick, R., He, K., Hariharan, B., Belongie, S.: Feature pyramid networks for object detection. In: Proceedings of the IEEE conference on computer vision and pattern recognition. pp. 2117–2125 (2017)
24. Liu, H., Liao, K., Lin, C., Zhao, Y., Guo, Y.: Pseudo-lidar point cloud interpolation based on 3d motion representation and spatial supervision. IEEE Transactions on Intelligent Transportation Systems (2021)
25. Liu, W., Anguelov, D., Erhan, D., Szegedy, C., Reed, S., Fu, C.Y., Berg, A.C.: Ssd: Single shot multibox detector. In: European conference on computer vision. pp. 21–37. Springer (2016)
26. Liu, Y., Wang, L., Liu, M.: Yolostereo3d: A step back to 2d for efficient stereo 3d detection. In: 2021 IEEE International Conference on Robotics and Automation (ICRA). pp. 13018–13024. IEEE (2021)
27. Loshchilov, I., Hutter, F.: Decoupled weight decay regularization. arXiv preprint arXiv:1711.05101 (2017)
28. Mai, N.A.M., Duthon, P., Khoudour, L., Crouzil, A., Velastin, S.A.: Sparse lidar and stereo fusion (sls-fusion) for depth estimationand 3d object detection. arXiv preprint arXiv:2103.03977 (2021)
29. Mao, J., Niu, M., Bai, H., Liang, X., Xu, H., Xu, C.: Pyramid r-cnn: Towards better performance and adaptability for 3d object detection. In: Proceedings of the IEEE/CVF International Conference on Computer Vision. pp. 2723–2732 (2021)
30. Mayer, N., Ilg, E., Hausser, P., Fischer, P., Cremers, D., Dosovitskiy, A., Brox, T.: A large dataset to train convolutional networks for disparity, optical flow, and scene flow estimation. In: Proceedings of the IEEE conference on computer vision and pattern recognition. pp. 4040–4048 (2016)
31. Park, D., Ambrus, R., Guizilini, V., Li, J., Gaidon, A.: Is pseudo-lidar needed for monocular 3d object detection? In: IEEE/CVF International Conference on Computer Vision (ICCV) (2021)
32. Qian, R., Garg, D., Wang, Y., You, Y., Belongie, S., Hariharan, B., Campbell, M., Weinberger, K.Q., Chao, W.L.: End-to-end pseudo-lidar for image-based 3d object detection. In: Proceedings of the IEEE/CVF Conference on Computer Vision and Pattern Recognition. pp. 5881–5890 (2020)

33. Redmon, J., Divvala, S., Girshick, R., Farhadi, A.: You only look once: Unified, real-time object detection. In: Proceedings of the IEEE conference on computer vision and pattern recognition. pp. 779–788 (2016)
34. Ren, S., He, K., Girshick, R., Sun, J.: Faster r-cnn: Towards real-time object detection with region proposal networks. Advances in neural information processing systems **28** (2015)
35. Roddick, T., Kendall, A., Cipolla, R.: Orthographic feature transform for monocular 3d object detection. arXiv preprint arXiv:1811.08188 (2018)
36. Rukhovich, D., Vorontsova, A., Konushin, A.: Imvoxelnet: Image to voxels projection for monocular and multi-view general-purpose 3d object detection. In: Proceedings of the IEEE/CVF Winter Conference on Applications of Computer Vision. pp. 2397–2406 (2022)
37. Scharstein, D., Hirschmüller, H., Kitajima, Y., Krathwohl, G., Nešić, N., Wang, X., Westling, P.: High-resolution stereo datasets with subpixel-accurate ground truth. In: German conference on pattern recognition. pp. 31–42. Springer (2014)
38. Shamsafar, F., Woerz, S., Rahim, R., Zell, A.: Mobilestereonet: Towards lightweight deep networks for stereo matching. In: Proceedings of the IEEE/CVF Winter Conference on Applications of Computer Vision. pp. 2417–2426 (2022)
39. Shi, S., Guo, C., Jiang, L., Wang, Z., Shi, J., Wang, X., Li, H.: Pv-rcnn: Point-voxel feature set abstraction for 3d object detection. In: Proceedings of the IEEE/CVF Conference on Computer Vision and Pattern Recognition. pp. 10529–10538 (2020)
40. Shi, S., Jiang, L., Deng, J., Wang, Z., Guo, C., Shi, J., Wang, X., Li, H.: Pv-rcnn++: Point-voxel feature set abstraction with local vector representation for 3d object detection. arXiv preprint arXiv:2102.00463 (2021)
41. Tian, Z., Shen, C., Chen, H., He, T.: Fcos: Fully convolutional one-stage object detection. In: Proceedings of the IEEE/CVF international conference on computer vision. pp. 9627–9636 (2019)
42. Vora, S., Lang, A.H., Helou, B., Beijbom, O.: Pointpainting: Sequential fusion for 3d object detection. In: Proceedings of the IEEE/CVF conference on computer vision and pattern recognition. pp. 4604–4612 (2020)
43. Wang, T., Xinge, Z., Pang, J., Lin, D.: Probabilistic and geometric depth: Detecting objects in perspective. In: Conference on Robot Learning. pp. 1475–1485. PMLR (2022)
44. Wang, T., Zhu, X., Pang, J., Lin, D.: Fcos3d: Fully convolutional one-stage monocular 3d object detection. In: Proceedings of the IEEE/CVF International Conference on Computer Vision. pp. 913–922 (2021)
45. Wang, Y., Chao, W.L., Garg, D., Hariharan, B., Campbell, M., Weinberger, K.Q.: Pseudo-lidar from visual depth estimation: Bridging the gap in 3d object detection for autonomous driving. In: Proceedings of the IEEE/CVF Conference on Computer Vision and Pattern Recognition. pp. 8445–8453 (2019)
46. Wang, Y., Yang, B., Hu, R., Liang, M., Urtasun, R.: Plumenet: Efficient 3d object detection from stereo images. In: 2021 IEEE/RSJ International Conference on Intelligent Robots and Systems (IROS). pp. 3383–3390. IEEE (2021)
47. Wang, Y., Guizilini, V.C., Zhang, T., Wang, Y., Zhao, H., Solomon, J.: Detr3d: 3d object detection from multi-view images via 3d-to-2d queries. In: Conference on Robot Learning. pp. 180–191. PMLR (2022)
48. Xu, S., Zhou, D., Fang, J., Yin, J., Bin, Z., Zhang, L.: Fusionpainting: Multimodal fusion with adaptive attention for 3d object detection. In: 2021 IEEE International Intelligent Transportation Systems Conference (ITSC). pp. 3047–3054. IEEE (2021)

49. Yoo, J.H., Kim, Y., Kim, J., Choi, J.W.: 3d-cvf: Generating joint camera and lidar features using cross-view spatial feature fusion for 3d object detection. In: European Conference on Computer Vision. pp. 720–736. Springer (2020)
50. You, Y., Wang, Y., Chao, W.L., Garg, D., Pleiss, G., Hariharan, B., Campbell, M., Weinberger, K.Q.: Pseudo-lidar++: Accurate depth for 3d object detection in autonomous driving. arXiv preprint arXiv:1906.06310 (2019)
51. Zbontar, J., LeCun, Y., et al.: Stereo matching by training a convolutional neural network to compare image patches. J. Mach. Learn. Res. **17**(1), 2287–2318 (2016)
52. Zhang, Y., Chen, Y., Bai, X., Yu, S., Yu, K., Li, Z., Yang, K.: Adaptive unimodal cost volume filtering for deep stereo matching. In: Proceedings of the AAAI Conference on Artificial Intelligence. vol. 34, pp. 12926–12934 (2020)
53. Zhou, X., Wang, D., Krähenbühl, P.: Objects as points. arXiv preprint arXiv:1904.07850 (2019)
54. Zhu, B., Jiang, Z., Zhou, X., Li, Z., Yu, G.: Class-balanced grouping and sampling for point cloud 3d object detection. arXiv preprint arXiv:1908.09492 (2019)